

Learning to Personalize in Appearance-Based Gaze Tracking

Erik Lindén

Tobii

elin@tobii.com

Jonas Sjöstrand

Tobii

jsjd@tobii.com

Alexandre Proutiere

KTH Royal Institute of Technology

alepro@kth.se

Abstract

In this paper, we investigate how to efficiently combine appearance-based methods and personal calibration for video-based gaze estimation. Previous calibration methods have learned an average model for all persons and then adapted it for a specific person. In contrast, we directly learn a model for personalized gaze estimation where the personal variations are modeled as a low-dimensional latent parameter space. During training, the network learns an efficient way to leverage these parameters for estimating gaze. After training, little person-specific data is required to optimize these (few) parameters. In fact, by calibrating only six parameters per person, the accuracy can be improved by a factor of up to 2.5, and reaches the same level as person-specific models.

We assess the performance of our method on Tobii’s large proprietary dataset, consisting of high resolution images taken from near-infrared cameras with active illumination. As it turns out, our method is the first appearance-based approach to gaze estimation to reach the same level of accuracy as involved model-based methods. We further demonstrate that it outperforms existing approaches on two datasets with relatively low-resolution images, MPIIGaze and GazeCapture. Finally, we show using a synthetic dataset created using UnityEyes tools, that our method efficiently predicts 3D gaze (origin and direction of gaze) without the need of explicitly 3D-annotated training data.

1. Introduction

Video-based gaze tracking deals with the problem of determining the gaze of a person’s eye given images of the eyes. By “gaze” one usually means the point on a two-dimensional screen where the person is looking (2D gaze), but sometimes one wishes to determine the complete gaze ray in 3D space, originating from the eye and directed towards the screen gaze point. We refer to this (five-dimensional) quantity as *3D gaze*. Gaze tracking has numerous applications: It is used as a communication aid for



Figure 1: Result on an average-performing recording in our dataset. This is a 19 inch screen. Green and red dots are predicted gaze points, crosses are gaze targets. Around each target, we show a circle corresponding to 3.9° , the best result on the MPIIGaze dataset [16, 22]. MPIIGaze uses similar screens, but is recorded with web cameras.

people with medical disorders. Experimental psychologists use it to study human behavior. In the consumer market, it is used for human-computer interaction and when used in virtual reality, it can reduce the computational requirements through foveated rendering, that is, rendering in high resolution only where the person is looking.

Gaze estimation techniques can be categorized into model-based and appearance-based methods [8]. Model-based methods use image features such as the pupil center and the iris edge, combined with a geometric eye model to estimate the gaze direction. Some model-based methods also use the corneal reflections from one or more light sources. These reflections are known as *glints* and the light sources are known as *illuminators*, typically light-emitting diodes. Model-based methods can be implemented with small amounts of training data, since they make simplifying assumptions. For example, they might model the pupil as a dark ellipse. However, the same assumptions make them unsuited to handle large variations in appearance.

Appearance-based methods, on the other hand, do not

rely on hand-crafted features. Instead, they estimate the gaze direction directly from the eye images. This requires a larger amount of training data, but makes it possible to track gazes despite appearance variations. Since appearance-based methods do not require an explicit feature-extraction step, they are believed to work better than model-based methods on low-resolution images [22]. Recent research on appearance-based methods using convolutional neural networks [2, 19, 12, 24, 23, 21, 3] has focused on challenging in-the-wild scenarios with person-independent models using low-resolution web camera images, and provided promising results.

In this paper, we propose a new approach to personal calibration in appearance-based 3D gaze tracking and analyze its performance both on low-resolution images and in more constrained scenarios, with high-resolution near-infrared cameras and active illumination. Figure 1 illustrates the spectacular improvements in accuracy the latter scenarios enable. The proposed 3D gaze estimation method consists of three steps: From the initial image of the face, we extract and normalize three images, two high-resolution images of the eyes, and one low-resolution image of the face. The three images resulting from the first step are fed into separate convolutional networks (corresponding to the convolutional part of ResNet-18 [9]). The final step combines the outputs of the networks and the calibration parameters tuned by letting the person look at known targets. Previous methods for personal calibration have trained person-specific models [22, 24] or seen calibration as a post-processing step [12]. This contrasts with our approach where we include calibration in the learning process, as a set of latent variables for each person.

Our method aims to predict gaze rays in 3D space. To make data collection simpler, we aim to learn this without explicitly annotating the 3D positions of the eyes in our training data. Instead we only use the 3D positions of the gaze targets. By predicting 3D gaze and having a generic personal calibration, we hope to learn a single model that can be used with different camera/screen geometries.

The method is evaluated using four datasets: Tobii’s large proprietary, consisting of high resolution images taken from near-infrared cameras with active illumination, the two datasets MPIIGaze and GazeCapture with lower resolution images, and a dataset consisting of synthetic images generated using UnityEyes tool to test the feasibility of 3D gaze predictions. These experiments demonstrate the following.

- Our appearance-based method with calibration achieves for the first time similar gaze accuracy as model-based methods on rich datasets(Tobii’s dataset).
- Our calibration significantly outperforms existing calibration approaches in both the MPIIGaze and

GazeCapture datasets. Our method actually yields gaze predictions of similar accuracy as person-specific models. Previous calibration methods have learned an average model for all persons and then adapted it for a specific person. We directly learn a model for personalized gaze estimation. We show that personal variations can be modeled as a low-dimensional latent parameter space, where little data is required for finding the optimal point for a given person.

- In the synthetic dataset created from UnityEyes tool, our method manages to accurately predict 3D gazes without explicit 3D annotations.

The contributions and outline of the paper are as follows: First, in Section 2, we review related work on appearance-based gaze tracking and approaches to personal calibration. In Sections 3 and 4, we describe our method and the datasets we used. The experimental results are found in Section 5. One of our results is that the personal variations can be modeled as a low-dimensional latent parameter space, and experiments suggest that it is enough to have about three parameters per eye. In Section 6, we argue why this is expected, inspecting typical model-based methods for gaze estimation. Finally, in Section 7, we discuss the implications of our results for appearance-based gaze tracking.

2. Related work

Appearance-based gaze tracking has received a lot of attention recently. Sugano *et al.* [18] used random forest regression to predict gaze angles from eye images. They introduced the normalization technique we adopt in this paper, where the eye images are warped into a normalized camera view. This effectively reduced the appearance variations their regressor needed to handle. For training, they augmented their dataset by rendering eye images from point clouds. Zhang *et al.* [22] introduced MPIIGaze, a dataset with more than 200 000 images from 15 persons. The dataset includes camera calibration parameters and 3D gaze targets. They trained a light-weight convolutional neural network to predicting gaze angles from eye images. Kraftka *et al.* [12] collected a dataset of almost 2.5 million images taken with smartphones in uncontrolled environments. They trained a convolutional neural network and without personal calibration they obtained an accuracy of about 3° (2 cm) on a phone or tablet. While the dataset is large, it lacks camera calibration parameters and 3D coordinates of the gaze targets. Wood *et al.* [20] introduced UnityEyes, a framework for generating synthetic eye images which look very realistic. With a k -nearest neighbor regressor, they obtained an accuracy of about 10° on the MPIIGaze dataset. Park *et al.* [15] used a novel heatmap approach to improve the regression performance, achieving 4.5° on MPIIGaze.

Fischer *et al.* [5] trained an ensemble of 4 VGG networks, which resulted in 4.3° on MPIIGaze.

2.1. Approaches to personal calibration

In model-based gaze tracking there is often some kind of personal calibration involved [8]. The personal parameters typically include the fovea offset for each eye, as discussed in Section 6. In appearance-based methods there is no explicit model of the eye, so it is not clear how to incorporate personal calibration. Most papers ignore calibration, though some authors have shown that person-specific estimators greatly outperform generic estimators.

For example, Sugano *et al.* [18] compared random forest regression with within-person training to the same method with cross-person training, finding errors of 3.9° and 6.5° . Zhang *et al.* [22] made the same comparison using a convolutional neural network on a different dataset, finding 3.3° versus 6.3° . Building on the idea of training person-specific estimators, Zhang *et al.* [21] devised a method which helped to collect more training data for a specific person.

A neural network trained for a specific person will of course always outperform a generic network, assuming equal amounts of training data. However, it is unpractical to collect the vast amount of data needed to train a modern neural network from a single person.

One approach to this problem is to retrain for each person not the complete network but only a part of it, typically the final layer. We adopt this approach as in Kafka *et al.* [12], but with a critical difference. In [12], the network is initially trained to learn an average model for all persons present in the dataset. The calibration is just a post-processing step where the last fully connected layer with input size 128 and output size 2 is replaced by an SVR-model trained with calibration samples for a specific person (while the weights of the rest of the network are kept fixed). With 13 calibration points, the accuracy was improved with up to 20 %, whereas with only 4 calibration points, the accuracy was actually worse than without personal calibration, probably due to overfitting of the SVR-model. In [12], personal calibration is learnt from scratch for each person. This requires a large calibration parameter space, to support a sufficiently rich set of calibration mappings, and hence a large number of calibration samples. This contrasts with our method: We parameterize the set of possible calibration mappings by a neural network, and during the initial training, the network learns a suitable mapping for a small calibration parameter space. The high expressiveness of the neural network means it can potentially model many different calibration mappings, and the training must find a suitable one. This necessitates a large training set, to prevent overfitting. We have this large dataset, since we learn the calibration mapping from the whole training set, not just from one person. This explains why our calibration method

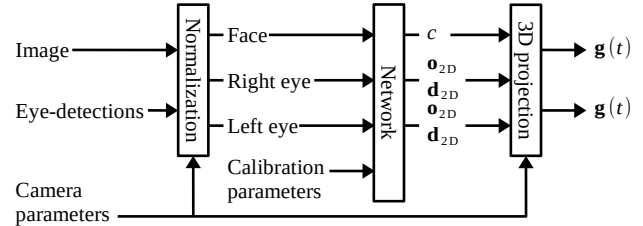


Figure 2: Network pre- and post-processing for image normalization and 3D gaze projection.

really outperforms the one of Kafka *et al.*

Park *et al.* [16] extended the method of Kafka *et al.* by extracting 32 landmarks (corresponding to iris edges, pupils, eyelids). These features are then used to train a personal SVR as in [12]. Our method also clearly outperforms the results presented in [16].

Finally it is worth mentioning Liu *et al.* [13]: The authors implemented personal calibration by training a differential neural network to predict the difference in gaze direction between two images. They then predicted the gaze angle difference between a set of calibration images and a novel image. Their accuracy was however no better than that of uncalibrated methods.

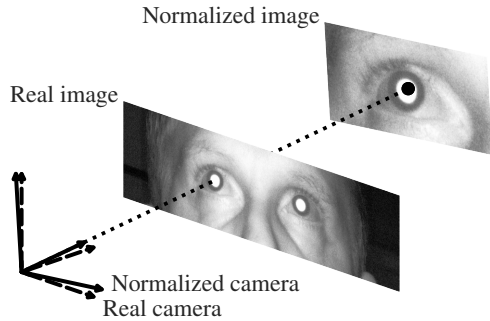
3. Method

In this section, we describe the three main components of our gaze prediction procedure: image normalization, the neural network and 3D gaze projection. See Figure 2 for an overview of the data flow. We also describe our personal calibration method.

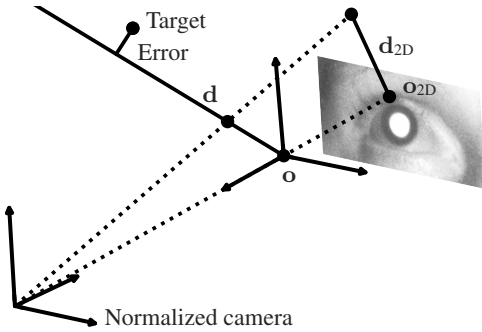
3.1. Image normalization

To improve generalization, we normalize the images as described in [18]. Unlike most other methods, we do not use a separate head pose algorithm for image normalization and 3D gaze prediction. We have found head pose algorithms to be fragile and they require pose-annotated training data. One of our datasets is also so tightly cropped to the eyes that most of the head is not visible. Instead we adopt a structure where eye detections are used for a rough pose estimation, for image normalization. The network is then asked to correct any errors (affecting gaze accuracy) in the rough estimate. The idea of head pose free methods has previously been investigated by [14, 3].

The input to the image normalization component is an image of a person's face and two points in the image defining where the eyes are. Those points are provided by an external eye detector. The output is three images: two high-resolution eye images centered at the eye detection points and one low-resolution face image centered at the midpoint between the eyes.



(a) Image normalization



(b) 3D gaze projection

Figure 3: (a) The image captured by the physical camera is warped into a normalized camera looking directly at the reference point, in this case the persons right eye. (b) The 2D gaze origin and gaze direction are combined with the corrected distance to form a gaze ray in 3D space. The miss distance between the gaze ray and the gaze target is the loss used to train the neural network.

By assuming that the face region has a short depth compared to the distance between the camera and the face, we can compensate for arbitrary scaling and camera rotation by a perspective image warp. This reduces the complexity of the gaze estimation problem, as the estimator does not need to handle arbitrary face rotations or scalings. However, due to imperfections in the normalization method, some rotation and scaling errors will remain.

Figure 3a illustrates the normalization. Given an input image \mathbf{I} and a reference point (either an eye detection point or the midpoint between the eyes), we compute a conversion matrix \mathbf{R} . Its inverse \mathbf{R}^{-1} is the matrix that rotates the camera so that it looks at the reference point and so that the interocular vector in the image becomes parallel to the camera x -axis. To make the eye appearance consistent, for the left-eye image we also let \mathbf{R}^{-1} mirror the camera in the interocular direction after the rotation.

The conversion matrix \mathbf{R} will map any 3D point in the real camera coordinate system into the normalized camera coordinate system. The same transform is applied to the image \mathbf{I} using an image transformation matrix $\mathbf{C}_n \mathbf{R} \mathbf{C}_r^{-1}$, where \mathbf{C}_r is the projection matrix of the real camera and \mathbf{C}_n is the projection matrix of the normalized camera. \mathbf{C}_n is selected as a scaling such that the interocular distance in the normalized image becomes 320 pixels for the eye images and 84 pixels for the face image. We use bilinear interpolation to implement the warping and crop out a $W \times H$ region in the normalized image, 224 \times 112 pixels for the eye images and 224 \times 56 pixels for the face image.

A gaze ray $\hat{\mathbf{g}}(t) = \mathbf{o} + t\mathbf{d}$ is estimated in the normalized camera coordinate system and transformed back to the real camera coordinate system by $\mathbf{g}(t) = \mathbf{R}^{-1}\hat{\mathbf{g}}(t)$.

3.2. 3D gaze projection

Here we describe how the output from the network is translated into a pair of 3D gaze rays. The network has five outputs. For each eye, it predicts a 2D gaze origin \mathbf{o}_{2D} and a 2D gaze direction \mathbf{d}_{2D} . It also predicts a distance correction term, c , which is common to both eyes. We assume that the distance from camera to eye is approximately the same for both eyes, and our estimate of it will be called ρ . First, given the input image and the eye detections, we find a rough distance ρ_{rough} such that the separation between the eyes becomes 63 mm at that distance, approximately the average human interocular distance [6]. This distance is then corrected by the network by letting $\rho = c \rho_{\text{rough}}$. The rough distance will be unreliable, since it is based only on the eye detections, which are noisy. Further, it makes no allowance for head yaw. But since the same eye detections are used to normalize the images fed to the network, the network has an opportunity to spot misaligned eye detections and correct for them. Likewise, it can measure the head yaw and correct for it.

We will now describe how a 3D gaze ray is computed for a single eye, see Figure 3b for an overview of the procedure. The 3D origin of the gaze ray, \mathbf{o} , is computed by back-projecting the 2D gaze origin \mathbf{o}_{2D} through the normalized camera to the distance ρ . To compute the 3D direction of the gaze ray, \mathbf{d} , we first construct a set of orthonormal basis vectors $\{\mathbf{x}, \mathbf{y}, \mathbf{z}\}$, where \mathbf{z} points from the 3D gaze origin to the camera and \mathbf{x} is orthogonal to the y -axis of the normalized camera coordinate system. The 3D gaze direction \mathbf{d} is then computed from the 2D gaze direction \mathbf{d}_{2D} as $\mathbf{d} = [\mathbf{x} \mathbf{y}] \mathbf{d}_{2D} + \mathbf{z}$.

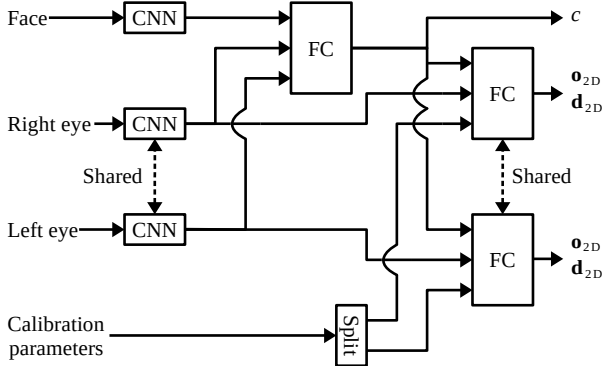


Figure 4: Network architecture.

3.3. Network architecture

Here we describe the input to the network and how the output is generated. See Figure 4 for an overview of the network architecture. We feed three images to the network: both eyes at high resolution and the face at low resolution. One convolutional network is applied separately to each eye. Another convolutional network is applied to the face. Both networks are the convolutional part of ResNet-18 [9].

The three outputs are concatenated and fed to a fully connected module. The fully connected module outputs the distance correction c . The rationale for using both the eyes and the face for the distance estimation, is that the eyes could provide accurate interocular distance measurements, while the face could improve head-pose estimation.

The convolutional network output for each eye is then concatenated with a set of N personal calibration parameters and the distance correction. This combined feature vector is fed to a fully connected module. The fully connected module outputs the 2D gaze origin \mathbf{o}_{2D} and the 2D gaze direction \mathbf{d}_{2D} . The same module is used for both eyes.

The fully connected modules can both be described as: FC(3072)-BN-ReLU-DO-FC(3072)-BN-ReLU-DO-FC(1 or 4) where FC is fully connected, BN is batch normalization [10] and DO is dropout [17].

Initially, we predicted the gaze origins and directions using information from both eyes. That gave better performance, but made the predictions for the two eyes highly correlated, as all training data have both eyes looking at the same point. As we want to support medical applications, where it is important to observe differences between the eyes, we choose this segregated approach. In a consumer application, it would be more appropriate to modify the network architectures to predict a joint gaze direction, originating from between the eyes, as suggested by Zhang *et al.* [23].

The rationale for providing the distance correction c when predicting the gaze direction is to allow the use of

features that require accurate distance information. This is the case with pupil-center/corneal-reflection gaze mapping [8, 7]. We do not input personal calibration parameters into the distance-estimation module, since it is typically impossible to detect distance errors from calibration data collected at a single distance, which is what we have.

3.4. Training and calibration

Personal variations are modeled by assigning $2N$ calibration parameters to each person, N for each eye. During training, the training set \mathcal{D} consists of triples (X, t, k) , where X is a triple of images (face, right eye, left eye), t is the 3D gaze target and k is the index of the person in the images. With K persons in the training set, we solve the optimization problem¹

$$(\theta_{\text{opt}}, P_{\text{opt}}) = \underset{\theta, P}{\operatorname{argmin}} \sum_{(X, t, k) \in \mathcal{D}} \text{loss}(g_{\theta}(X, P_{k, \cdot}), t)$$

over all K -by- $2N$ matrices P of calibration parameters and, simultaneously, over all possible parameters θ of the network g . After training, P_{opt} is discarded. The optimization method and the loss function will be described in a moment.

To calibrate for a new person, we collect a small calibration set \mathcal{D}_{cal} of (image triple, gaze target) pairs. The calibration procedure then finds the person's $2N$ calibration parameter vector defined as

$$\underset{p \in \mathbb{R}^{2N}}{\operatorname{argmin}} \sum_{(X, t) \in \mathcal{D}_{\text{cal}}} \text{loss}(g_{\theta_{\text{opt}}}(X, p), t).$$

Note that the network weights are fixed. We used gradient descent to solve this optimization problem, starting from the zero vector. Since the space \mathbb{R}^{2N} of possible calibration parameter vectors is so low-dimensional, this can be done quickly, and we did not see any problem with local minima.

In the experiments, we vary N and find that 3 parameters per eye are enough to provide an efficient person-specific gaze estimation. Modeling personal variations using such a low-dimensional latent parameter space contrasts with existing calibration approaches (e.g. in [12], a much higher number of parameters is used), but can be motivated and justified by inspecting existing model-based methods; see Section 6 for a complete discussion.

Finally, let us describe the loss function and the optimization method during training. The loss is the miss distance between the gaze ray and the 3D gaze target, see Figure 3b. We train using Adam [11] with a learning rate of 10^{-3} . The eye detections are jittered for data augmentation in training, but not in test. Specifically, we randomly offset the detections in a disk with a radius equal to 4 % of

¹Note that our objective function includes person-specific parameters P_k , which contrasts with existing methods [12] whose objective function does not account for personal variations (with our notations, it would be $\sum_{(X, t) \in \mathcal{D}} \text{loss}(g_{\theta}(X))$).

the interocular distance. The test results are reported on the model with the lowest validation error.

With this setup, we found that the predicted gaze rays would pass close to the gaze target, but the 3D gaze origin would be highly incorrect. The reason is that current datasets are collected with a geometrical setup that makes the 3D gaze origin underdetermined. In the supplementary material we use a synthetic dataset to investigate whether this limitation can be overcome by a different data collection strategy.

To prevent unphysical solutions when training on current datasets, we introduced two regularizing terms. First, a hinge loss on the 2D gaze origin \mathbf{o}_{2D} , penalizing if it moves outside the eye image. Secondly, a hinge loss on the distance correction c , penalizing changes in distance by more than 40 % in either direction.

4. Datasets

We use three datasets in our experiments: an internal dataset at Tobii with near-infrared illumination and the MPIIGaze and GazeCapture datasets. In the supplementary material we also investigate the effect of gaze target placement and glints on a synthetic UnityEyes dataset.

4.1. NIR dataset

We use a large internal dataset at Tobii for our calibration experiments. The dataset was collected with a professional eye tracker platform, with an infrared illuminator mounted very close to the camera. This produces a bright-pupil effect [8], the same effect that makes the eyes red in flash photography. Since the illuminator position coincides with the camera position, we can scale and rotate the normalized camera without changing the position of the illuminator in the camera coordinate system. The training subset was collected over a period of several years and contains 426 535 images from 1824 persons. The majority of the training data have gaze targets on a regular lattice.

For validation and testing, we have two subsets with 200 persons each (these persons were not present in the training data). These subsets were collected on 19 inch, 16:10 aspect ratio screens, with the camera placed at the bottom edge of the screen and tilted up 20°. The camera focal length was 3679 pixels and it captured a region of interest of 1150 × 300 pixels. The region of interest was kept aligned on the eyes using an eye detector. The persons sat at 65 ± 10 cm from the camera. See Figure 3a for an example image. Half of the recordings were made in Sweden, the other half in China.

There are three recordings for each person, one for calibration and two for test. From each recording, we extract 45 images, evenly distributed over gaze targets. The calibration recordings have gaze targets on a regular 3×3 lattice. For the test recordings, the screen was divided into a

3×4 grid and a gaze target was placed randomly in each grid cell. The screen brightness was also randomized. For validation and testing, we first calibrate on the calibration recording and then report the error on the two test recordings. As the setup was quite controlled, we believe head yaw angles were on the order of 10°.

4.2. MPIIGaze dataset

We use the MPIIGaze dataset [24] to compare our method to existing approaches. MPIIGaze contains images of 15 persons, captured while they were viewing their laptop screens by the laptop camera. As the dataset is small, we do leave-one-person-out experiments [22, 24], that is, we train on 14 persons and test on one person, repeating 15 times. We use a variant of MPIIGaze which is similar to the one used by Zhang *et al.* [23], which is similar to MPIIGaze+ of [24]. In MPIIGaze+, the annotations from the original MPIIGaze [22] have been improved, but MPIIGaze+ is not fully public; the public MPIIGaze is cropped to the original eye detections, so in some cases, the eyes are not visible in the cropped images.

We use the publicly available MPIIGaze with the annotations from MPIIGaze+, but discard an image if any eye detection has moved more than 25 % of the original interocular distance. That leaves 36 965 images, 98 % of MPIIGaze+. For full-face gaze estimation, like ours, Zhang *et al.* [23] mirrored the image when MPIIGaze had two eyes from the same image, to get a total of 3000 face images per person. Our calibration does not support mirroring, so we first compute the mean error for each person, over whatever number of images that are available, and then take the average of those means. For our calibrated network, we calibrate on 100 randomly selected images, and test on the rest.

4.3. GazeCapture dataset

The GazeCapture dataset was collected by Krafka *et al.* [12]. It contains 1 490 959 images from 1471 persons, collected on iPhones and iPads. It does not provide camera calibrations, and the gaze targets are assumed to lie in the image plane of the camera. To apply our method, we assume that all cameras have a horizontal field-of-view of 54.4° [1] and that the principal point is always in the middle of the image.

As the eye detections often are quite off, we increase the area viewed by our eye crop by 50 %. This makes most, but not all, eyes visible. To make our results comparable to those of Krafka *et al.*, we clamp our predicted gaze points to the screen area of the device and take the mean gaze point of both eyes, before measuring the Euclidean distance to the target. We split off the first 13 points (per device orientation) for calibration on the test set. We leave all those points out even when calibrating on fewer points.

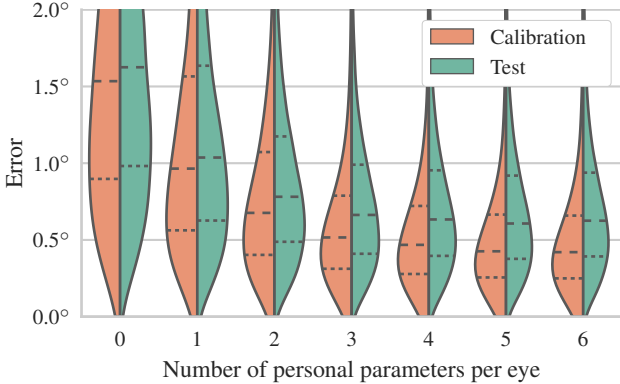


Figure 5: Distribution of angle errors as a function of the number of calibration parameters per eye on the NIR dataset. Dashed lines show quartiles.

5. Experiments

While we minimize the gaze-ray miss distance, we report the error as an angle for easier comparison with previous work. For the NIR dataset, where we have no ground truth, we assume that all eyes are at a distance of 65 cm from the camera. For the MPIIGaze dataset, we use the provided 3D eye positions to compute an angular error. While it is common to report the performance as the mean error, since we have found that user interface design tends to be driven by the worst-case errors, we plot the full distribution of errors.

5.1. NIR dataset

Impact of the number of calibration parameters. We vary the number N of calibration parameters per eye and report the error on the calibration recordings and on the test recordings, see Figure 5. We want to point out that the absence of calibration does not add a fixed drop in performance compared with the calibrated case, but rather a scaling. In particular, we find that any given quantile of the error is approximately 2.5 times higher for $N = 0$ (uncalibrated) than for $N = 3$. As $N = 3$ seems to provide near optimal performance, we use that for all other experiments. The mean error is 0.8° , which compares well with multi-camera, multi-illuminator systems [8, 4].

Impact of the dataset size. To investigate the impact of large-scale data, we subsample persons in the training set. The validation and test sets are unchanged. This experiment is similar to one performed by Kafka *et al.* [12]. The results are shown in Figure 6. Like Kafka *et al.*, we find that a large training set significantly improves the performance.

Kafka *et al.* also compared the importance of having samples from many persons with the importance of having many samples per person. We cannot do this experiment, as each person in our dataset only looked at about 27 targets.

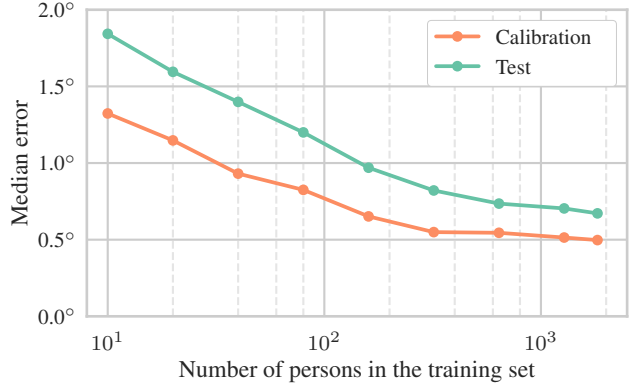


Figure 6: Angle error as a function of the training set size on the NIR dataset.

Method	Mean error ($^\circ$)
GazeNet+ [24]	5.4
Uncalibrated CNN [ours]	5.1
Spatial weights CNN [23]	4.8
*Differential CNN [13]	4.7
Pictorial CNN [15]	4.5
RT-GENE [5]	4.3
*Landmark CNN [16]	3.9
*Calibrated CNN [ours]	2.6
GazeNet+ (person-specific) [24]	2.5

Table 1: Results on the MPIIGaze dataset. Most values are not directly comparable, see the text for details. * indicates a calibrated method.

While we do have multiple images per target, those images are highly correlated. This also means that the NIR dataset is significantly different from the MPIIGaze dataset: The former has many persons with few samples, the latter has few persons with many samples.

5.2. MPIIGaze dataset

We compare our calibrated neural network with other methods on the MPIIGaze dataset, see Table 1. In the last line of the table, we further report the performance of a method where the entire network is specifically trained for each person (the person-specific CNN is trained on 2500 images and tested on 500 images). Also note that we also train an uncalibrated model (zero calibration parameters) to disentangle the improvement due to calibration from other architectural differences.

The results for the different methods are not directly comparable, as their configurations differ depending on the

Method	Calibration points	Mean error (cm)	
		Phone	Tablet
iTracker*	0	1.71	2.53
Uncalibrated CNN		1.61	2.46
iTracker*	4	1.65	3.12
Calibrated CNN		1.29	1.76
iTracker*	13	1.34	2.12
Calibrated CNN		1.26	1.74

Table 2: Results on GazeCapture. The iTracker* method is by [12] and the (un)calibrated CNN is our method.

way annotations may have been improved, on whether externally provided head pose is used, on whether only one eye or the whole face is used, and on which subsets of training and test images are used.

We see that our CNN with a low-dimensional personal calibration, three parameters per eye, performs much better than generic CNNs, and is even comparable to the person-specific CNN. The error for our uncalibrated model is about 1.9 times as high as the error for our calibrated model.

Since the MPIIGaze dataset is so small, only 15 persons, it is not a reliable metric for constructing a definitive ranking of gaze estimation methods. We do believe, however, that these results support the idea that personal variations are well-described by a low-dimensional latent parameter space.

5.3. GazeCapture dataset

The results on GazeCapture are shown in Table 2. We compare our method to iTracker* [12], the only other method on GazeCapture that we know of. The iTracker* method uses SVR for calibration and has a fine-tuned model for each device and orientation. Our method consistently outperforms iTracker*, even though we use the same model for all devices and orientations.

Since our method only calibrates a total of 6 personal parameters, it calibrates almost as well with 4 points as with 13 points, whereas iTracker* calibrates 256 parameters and performs significantly worse when calibrated with only 4 points. Calibration improves the performance by a factor of 1.3 for phones and 1.4 for tablets.

6. Low-dimensional parameter space for calibration: the case of model-based methods

To understand why it is reasonable to model personal variations as a low-dimensional latent parameter space, it helps to look at a typical model-based method for gaze

tracking. Here we will review the eye model described by Guestrin and Eizenman [7]. For a comprehensive review of model-based methods, we refer to [8].

We will describe a gaze mapping model called pupil-center/corneal-reflection, or *PCR*. Assume a system with one camera and a collocated illuminator. Further assume we know the distance to the eye, from head pose estimation, a second stereo camera or some other method.

Image processing methods detect the corneal reflection, the glint, from the illuminator. The center of the pupil is also detected. The difference between these two points forms the pupil-center/corneal-reflection vector. If the cornea is assumed to be spherical, the cornea center lies directly behind the glint. The *optical axis*, a line passing through the cornea center and the pupil center, can then be computed if the distance between the person’s cornea center and pupil center is known. This distance is one personal parameter.

However, the optical axis is not the *visual axis*, the person’s line of gaze. The fovea, the most sensitive part of the retina, is offset from the optical axis, and this offset, in two dimensions, differs from person to person.

Taken together, we have three parameters per eye for each person. The foveal offset roughly corresponds to shifting the gaze up-and-down and side-to-side, and the cornea-center/pupil-center distance scales the gaze around the optical axis.

Over the three datasets, NIR, MPIIGaze and GazeCapture, the GazeCapture dataset sees the least improvement from calibration, and the NIR dataset sees the greatest. The former also has the worst images, while the latter has the best. We do not believe that this is a coincidence. As measurement errors in the images decrease, the mismatch between a generic gaze estimation model and a specific person’s eye geometry becomes the dominant source of errors.

7. Conclusions

We propose a way to incorporate personal calibration into a deep learning model for video-based gaze estimation. Using our method, we show that an appearance-based gaze tracking system with a single camera and a collocated illuminator can achieve accuracy similar to model-based, multi-camera, multi-illuminator systems.

The number of calibration parameters is low, about three per eye, and similar to the number predicted by geometrical models. When evaluated on the MPIIGaze dataset, our estimator performs better than deep learning methods with person-specific models.

Experiments on synthetic data (in the supplementary material) suggest it would be possible to learn accurate 3D gaze (both origin and direction of gaze) without annotated eye positions.

Acknowledgement This work was partially supported by the Wallenberg AI, Autonomous Systems and Software Program (WASP) funded by the Knut and Alice Wallenberg Foundation

References

- [1] Apple Inc. iOS Device camera summary. Available at <https://developer.apple.com/library/archive/documentation/DeviceInformation/Reference/iOSDeviceCompatibility/Cameras/Cameras.html>. 6
- [2] S. Baluja and D. Pomerleau. Non-intrusive gaze tracking using artificial neural networks. In J. D. Cowan, G. Tesauro, and J. Alspector, editors, *Advances in Neural Information Processing Systems 6*, pages 753–760. Morgan-Kaufmann, 1994. 2
- [3] H. Deng and W. Zhu. Monocular free-head 3D gaze tracking with deep learning and geometry constraints. In *2017 IEEE International Conference on Computer Vision (ICCV)*, pages 3162–3171, Oct. 2017. 2, 3
- [4] O. Ferhat and F. Vilario. Low cost eye tracking: The current panorama. *Computational Intelligence and Neuroscience*, page 14, 2016. 7
- [5] T. Fischer, H. Jin Chang, and Y. Demiris. RT-GENE: Real-time eye gaze estimation in natural environments. In *The European Conference on Computer Vision (ECCV)*, September 2018. 3, 7
- [6] C. C. Gordon, C. L. Blackwell, B. Bradtmiller, J. L. Parham, P. Barrientos, S. P. Paquette, B. D. Corner, J. M. Carson, J. C. Venezia, B. M. Rockwell, M. Mucher, and S. Kristensen. 2012 Anthropometric survey of U.S. Army personnel: Methods and summary statistics. Technical Report NATICK/15-007, Natick MA: U.S. Army Natick Soldier Research, Development and Engineering Center, 2014. 4
- [7] E. D. Guestrin and M. Eizenman. General theory of remote gaze estimation using the pupil center and corneal reflections. *IEEE Transactions on Biomedical Engineering*, 53(6):1124–1133, June 2006. 5, 8
- [8] D. W. Hansen and Q. Ji. In the eye of the beholder: A survey of models for eyes and gaze. *IEEE Transactions on Pattern Analysis and Machine Intelligence*, 32(3):478–500, 2010. 1, 3, 5, 6, 7, 8
- [9] K. He, X. Zhang, S. Ren, and J. Sun. Deep residual learning for image recognition. *CoRR*, abs/1512.03385, 2015. 2, 5
- [10] S. Ioffe and C. Szegedy. Batch normalization: Accelerating deep network training by reducing internal covariate shift. In *Proceedings of the 32Nd International Conference on International Conference on Machine Learning - Volume 37*, ICML’15, pages 448–456. JMLR.org, 2015. 5
- [11] D. P. Kingma and J. Ba. Adam: A method for stochastic optimization. *CoRR*, abs/1412.6980, 2014. 5
- [12] K. Kafka, A. Khosla, P. Kellnhofer, H. Kannan, S. Bhandarkar, W. Matusik, and A. Torralba. Eye tracking for everyone. In *IEEE Conference on Computer Vision and Pattern Recognition (CVPR)*, 2016. 2, 3, 5, 6, 7, 8
- [13] G. Liu, Y. Yu, K. A. Funes Mora, and J.-M. Odobez. A differential approach for gaze estimation with calibration. In *29th British Machine Vision Conference*, 2018. 3, 7
- [14] F. Lu, T. Okabe, Y. Sugano, and Y. Sato. A head pose-free approach for appearance-based gaze estimation. In *British Machine Vision Conference, BMVC 2011, Dundee, UK, Au-*

gust 29 - September 2, 2011. Proceedings, pages 1–11, 2011.

3

- [15] S. Park, A. Spurr, and O. Hilliges. Deep pictorial gaze estimation. In *The European Conference on Computer Vision (ECCV)*, September 2018. 2, 7
- [16] S. Park, X. Zhang, A. Bulling, and O. Hilliges. Learning to find eye region landmarks for remote gaze estimation in unconstrained settings. In *Proc. International Symposium on Eye Tracking Research and Applications (ETRA)*, pages 21:1–21:10, 2018. 1, 3, 7
- [17] N. Srivastava, G. Hinton, A. Krizhevsky, I. Sutskever, and R. Salakhutdinov. Dropout: A simple way to prevent neural networks from overfitting. *J. Mach. Learn. Res.*, 15(1):1929–1958, Jan. 2014. 5
- [18] Y. Sugano, Y. Matsushita, and Y. Sato. Learning-by-synthesis for appearance-based 3D gaze estimation. In *2014 IEEE Conference on Computer Vision and Pattern Recognition*, pages 1821–1828, June 2014. 2, 3
- [19] K.-H. Tan, D. J. Kriegman, and N. Ahuja. Appearance-based eye gaze estimation. In *Proceedings of the Sixth IEEE Workshop on Applications of Computer Vision, WACV '02*, pages 191–, Washington, DC, USA, 2002. IEEE Computer Society. 2
- [20] E. Wood, T. Baltrušaitis, L.-P. Morency, P. Robinson, and A. Bulling. Learning an appearance-based gaze estimator from one million synthesised images. In *Proceedings of the Ninth Biennial ACM Symposium on Eye Tracking Research & Applications*, pages 131–138, 2016. 2
- [21] X. Zhang, M. X. Huang, Y. Sugano, and A. Bulling. Training person-specific gaze estimators from interactions with multiple devices. In *Proc. ACM SIGCHI Conference on Human Factors in Computing Systems (CHI)*, 2018. 2, 3
- [22] X. Zhang, Y. Sugano, M. Fritz, and A. Bulling. Appearance-based gaze estimation in the wild. In *Proc. of the IEEE Conference on Computer Vision and Pattern Recognition (CVPR)*, pages 4511–4520, June 2015. 1, 2, 3, 6
- [23] X. Zhang, Y. Sugano, M. Fritz, and A. Bulling. It’s written all over your face: Full-face appearance-based gaze estimation. In *2017 IEEE Conference on Computer Vision and Pattern Recognition Workshops (CVPRW)*, pages 2299–2308, July 2017. 2, 5, 6, 7
- [24] X. Zhang, Y. Sugano, M. Fritz, and A. Bulling. MPIIGaze: Real-world dataset and deep appearance-based gaze estimation. *CoRR*, abs/1711.09017, 2017. 2, 6, 7

Learning to Personalize in Appearance-Based Gaze Tracking: Supplementary Material

Erik Lindén

Tobii

elin@tobii.com

Jonas Sjöstrand

Tobii

jsjd@tobii.com

Alexandre Proutiere

KTH Royal Institute of Technology

alepro@kth.se

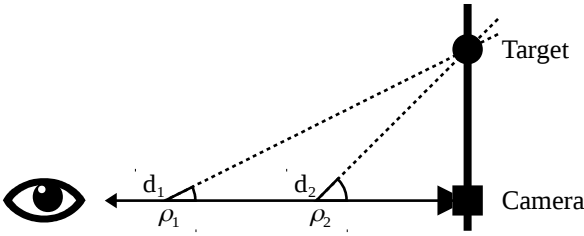


Figure 1: When the eyes lie along the z -axis of the camera and the gaze targets are in the image plane of the camera, there are multiple combinations of distance and gaze direction that minimize the error.

UnityEyes

The NIR, MPIIGaze and GazeCapture datasets all have all gaze targets in the same plane (approximately the camera image plane). We found that this makes it impossible to learn meaningful gaze origins, see Figure 1. The network can always compensate for an incorrect origin by modifying the gaze direction. The gaze ray will still pass through the gaze target, but the ray is only correct at that point. However, if gaze targets are placed at various z -depths in the camera coordinate system, it is no longer possible to compensate origin errors by changing the gaze direction. The reason is that there will be pairs of well separated gaze targets corresponding to nearly identical input images to the network. By continuity, the corresponding pair of gaze ray predictions are almost identical, and the error is minimized only when that predicted gaze ray almost passes through both gaze targets.

The gaze origins could be learned directly from data on the position of the eyes, but in practice we find it difficult to design a data collection setup where we can measure the position of eyes with the necessary accuracy, which is on the order of millimeters.

To test the feasibility of learning 3D gaze without ground-truth eye positions, we generate synthetic images

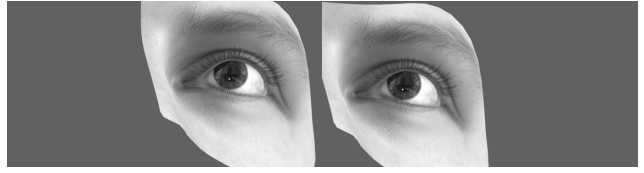


Figure 2: UnityEyes composition.

using the UnityEyes tool [3]. This lets us place gaze targets at different depths. The dataset defines gaze in terms of the *optical axis* of the eye [2], so we use no personal calibration.

We make the synthetic images similar to the NIR dataset, with the camera 20° below the face and with gaze points above the camera. Relative to the camera, the gaze angle range is 0° to 40° in pitch and $\pm 40^\circ$ in yaw. The head pose range is 10° to 30° in pitch and $\pm 20^\circ$ in yaw. Specifically, we set the fields in the tool to $[-20, 0, 10, 20]$ and $[0, 0, 10, 20]$. Since we know the geometry of the eye surface, we have the opportunity to add glints from a coaxial light source. We generate one million UnityEye images and split 80/10/10 for training/validation/test. To reduce compression artifacts, we generate the images at 1024×768 pixels and rescale them to match the camera of the NIR dataset.

The eyes are placed at 65 cm, with gaze targets randomly placed at a z -depth of one of -30 , 0 and $+30$ cm. We sample the interocular distance from $\mathcal{N}(63 \text{ mm}, 3.5^2 \text{ mm}^2)$ [1]. See Figure 2 for an example image. We use the center of the eyelid annotations as the eye detections. To make the detections less perfect, we randomly offset them in a circular disk with a radius equal to 3 % of the interocular distance.

Results

The results are shown in Figure 3. We see that the 2D training data result in very large errors. This was also reflected in the distances between predicted gaze rays and true gaze origins. On this synthetic data, we see that glints do improve the accuracy by a small factor.

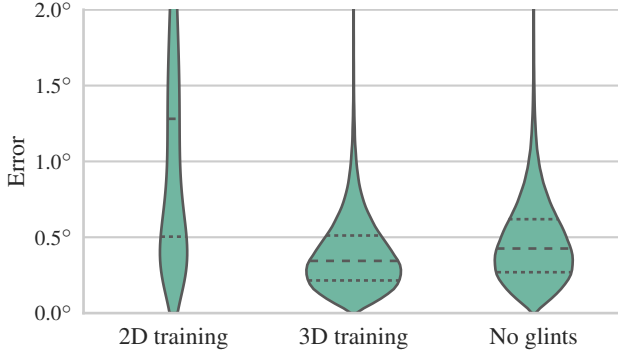


Figure 3: Distribution of angle errors on the UnityEyes dataset. *2D training* has all gaze targets in the same plane. For *3D training*, the gaze targets are distributed among three planes. *No glints* also has the gaze targets in three planes, but in this case no glints were added to the images. In all cases, the test data has gaze targets in three planes. Dashed lines show quartiles.

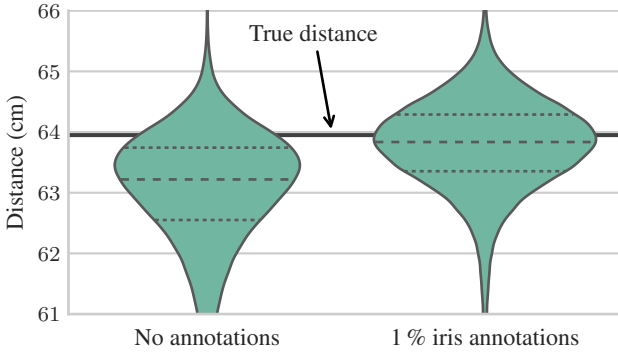


Figure 4: Distribution of estimated distances to the iris on the UnityEyes dataset, with and without iris annotations. Dashed lines show quartiles.

While the predicted gaze rays as such are close to the true gaze origins, there is nothing forcing the predicted gaze origins to coincide with any physical feature on the eye, and the origins tend to be “floating” along the gaze ray. In an attempt to improve the prediction, we used iris metadata to annotate a 1 % subset of the UnityEyes image with iris centers. We then added an additional term to the cost function, an L^2 loss on the distance between the iris center and the 2D gaze origin. The distances to the predicted gaze origins are shown in Figure 4. We see that sparse iris annotations improves the consistency of the distance estimate.

References

[1] C. C. Gordon, C. L. Blackwell, B. Bradtmiller, J. L. Parham, P. Barrientos, S. P. Paquette, B. D. Corner, J. M. Carson, J. C. Venezia, B. M. Rockwell, M. Mucher, and S. Kristensen. 2012 Anthropometric survey of U.S. Army personnel: Methods and summary statistics. Technical Report Natick/15-007, Natick MA: U.S. Army Natick Soldier Research, Development and Engineering Center, 2014. [1](#)

[2] D. W. Hansen and Q. Ji. In the eye of the beholder: A survey of models for eyes and gaze. *IEEE Transactions on Pattern Analysis and Machine Intelligence*, 32(3):478–500, 2010. [1](#)

[3] E. Wood, T. Baltrušaitis, L.-P. Morency, P. Robinson, and A. Bulling. Learning an appearance-based gaze estimator from one million synthesised images. In *Proceedings of the Ninth Biennial ACM Symposium on Eye Tracking Research & Applications*, pages 131–138, 2016. [1](#)